IMR Press

Original Research

Molecular imaging diagnosis of atherosclerotic vulnerable plaque in rabbit carotid artery using a self-assembled nanoscale ultrasound microbubble contrast agent

Cong Wang[1], Shaoling Yang[2,3,*], Xiaoxue Chen[3], Qianqian He[3], Kun Zhao[3], Jing Hu[3]

[1] *Department of Ultrasound, The First Hospital of Anhui University of Science and Technology, 232007 Huainan, Anhui, China*

[2] *Department of Ultrasound, The Eighth People's Hospital of Shanghai, 200235 Shanghai, China*

[3] *Department of Cardiovascular Ultrasound, Affiliated Hospital of Anhui University of Science and Technology, 201406 Shanghai, China*

*Correspondence: dryslfx@163.com (Shaoling Yang)

DOI:10.31083/j.rcm2204173

Submitted: 23 August 2021 Revised: 12 October 2021 Accepted: 12 October 2021 Published: 22 December 2021

This study aimed to prepare an anti-Vascular cell adhesion protein 1 (VCAM-1) nanoscale ultrasound microbubble contrast agent using the hyperbranched self-assembly method for the molecular imaging diagnosis of atherosclerotic vulnerable plaques in rabbits. Twenty-five rabbits with carotid atherosclerosis were randomly divided into 5 groups, and the ear vein was injected with agents as follows: Groups A and B: nanoscale ultrasound microbubble contrast agent with and without anti-VCAM-1 agent; Groups C and D: SonoVue ultrasonic microbubble contrast agent, with and without anti-VCAM-1 agent; Control group: saline. The molecular imaging diagnosis of the atherosclerotic plaque, involved the examination of its vulnerability in the rabbit carotid artery was performed using the contrast ultrasound mode. The arrival and peaking time of the anti-VCAM-1 nanoscale ultrasound microbubble contrast agent (Group A) for plaque occurred earlier than those of the other groups ($p < 0.05$), and with it, the plaque showed the strongest enhancement ($p < 0.05$), followed by the SonoVue ultrasound microbubble contrast agent with anti-VCAM-1 group (Group C) and the self-made nanoscale ultrasound microbubble contrast agent group (Group B). No development was observed in the plaques of the SonoVue ultrasound microbubble contrast agent group and the control group. The anti-VCAM-1 nanoscale ultrasonic microbubble contrast agent, prepared using the self-assembly method, can facilitate the development effect of the carotid atherosclerotic vulnerable plaque, providing a basis for the molecular imaging diagnosis of carotid atherosclerotic vulnerable plaques.

Keywords

Vulnerable plaque; Targeted; Microbubble; Anti-VCAM-1

1. Introduction

Stroke is the second leading cause of death due to cardiovascular and cerebrovascular diseases globally. Previous studies have reported that two important causes of ischemic stroke are occlusive stenosis and plaque rupture with associated thrombosis [1–3]. At present, there is no effective method for evaluating the susceptibility of atherosclerotic plaques to rupture [4, 5]. Thin fibrous cap, large lipid-rich necrotic cores, neovascularization, high infiltration of inflammatory cells, and plaque-related thrombosis are important for judging the susceptibility of an atherosclerotic plaque to rupture [6]. Neovascularization runs through the entire course of atherosclerotic plaque formation and development. New blood vessels are mostly composed of monolayer endothelial cells characterized by the lack of tight connections, poor continuity of the basement membrane, and lack of connective tissue, which provides support around the blood vessels, so they are brittle and permeable [7]. Inflammatory cells and fatty substances are more likely to infiltrate the plaque through gaps in the new blood vessels, leading to an inflammatory response within the plaque [8]. When the plaque is too large, ischemia and hypoxia occur easily, and the rupture of new blood vessels leads to intra-plaque bleeding [9]. This leads to a rapid increase in the volume of plaque and damage or rupture of the plaque surface [10]. These rupture-prone plaques are called "vulnerable plaques". Therefore, neovascularization is a landmark characteristic of susceptibility to vulnerable plaques, and the detection of neovascularization in plaques guides clinical treatment. Neovascularization is difficult to detect using commercially available micron-scale ultrasound contrast media because of the extremely small diameter and tortuosity of the endothelial cells. Qualitative diagnosis of vulnerable plaques is still difficult at this stage.

Vascular cell adhesion molecule (VCAM)-1 is expressed by activated endothelial cells and plays a role in leukocyte rolling and adhesion by interacting with its receptor very late antigen-4 (VLA-4) on monocytes and lymphocytes [11, 12]. It has been reported that inflammatory activation of the endothelium, involving upregulation of VCAM-1, promotes the recruitment of monocytes into the arterial wall, precedes plaque formation, and plays a role in the occurrence and progression of plaque [12, 13]. Therefore, imaging techniques that assess changes in VCAM-1 expression could be utilized to determine the risk of atherosclerosis-related events [14, 15]. However, the short circulation time (minutes) and relatively large size (two–ten micrometers) of currently used microbubbles do not allow effective extravasation into tissue, preventing efficient targeting [16, 17]. Therefore, this study aimed to investigate the binding ability of self-made nanoscale microbubbles and VCAM-1 and compare the effects of self-made nanoscale microbubble contrast agent and SonoVue contrast agent on plaque ultrasound imaging. Accurate diagnosis of vulnerable plaques based on cellular and molecular imaging is predicted to guide the long-term clinical management and treatment options for high-risk stroke patients.

2. Materials and methods

2.1 Preparation of carotid atherosclerotic plaque in rabbits and ultrasound examination

Forty adult male New Zealand white rabbits aged 3–5 months, with large ears and body mass of 2.0–2.5 kg, were provided by the Shanghai Fengxian Tengda Rabbit Industry [SCXK (Shanghai) 2014-0003]. The rabbits were fed under natural light, with alternating day and night cycles and unlimited drinking water. Each rabbit was kept in one cage and singly fed. Modeling experiment group (34 rabbits) were provided with high-fat diet (formula: 74.5% regular feed, 10% lard, 0.5% cholesterol, 10% egg yolk powder, 5% sucrose); 100 g daily for each rabbit. The control group (6 rabbits) were fed normally.

34 rabbits were used to construct a rabbit carotid atherosclerotic plaque model. The rabbit carotid atherosclerosis model was established by referring to the method of using high-fat feeding and modified silicone rubber ring reported by Li *et al.* [18]. Briefly, the left common carotid arteries were separated from the surrounding connective tissue after rabbits were anesthetized with 3 percent sodium pentobarbital. The left common carotid artery was sheathed with a silicone collar, and the collar-opening was closed with an adhesive until the end of the experiment. The skin was sutured after the opening was firmly closed.

Blood (2 mL) of was sampled from the auricular vein at week 0, week 4, week 8, and week 12 and centrifuged at a speed of 1118 g per 3–5 min at 4 °C. Red blood cell was discarded and plasma was centrifuged at a speed of 6440 g per 5 min. The expressions of triglycerides, cholesterol, and low-density lipoprotein in the supernatant were measured by enzyme linked immunosorbent assay (ELISA) method (Rabbit Triglyceride ELISA Kit, JL17061, J&L Biological Technology Co., Ltd. Shanghai, China; Rabbit Total Cholesterol ELISA Kit, JL16914, J&L Biological Technology Co., Ltd., Shanghai, China; Rabbit Low Density Lipoprotein ELISA Kit, JL17065, J&L Biological Technology Co., Ltd, Shanghai, China).

Ultrasound examination of the common carotid artery in the rabbits was performed at 4, 8, and 12 weeks after surgery. The rabbits were anesthetized and immobilized, and the hair of the rabbits on the neck was shaved, with the head turned opposite to the side of the examination. The GE Vivid E9 ultrasound scanner (GE Healthcare Co., Milwaukee, WI, USA) with a line-of-array probe (8–10 MHz) was used for ultrasound examination. The scanning depth was adjusted to 3 cm, the grayscale gain was adjusted to 53%, and the two-dimensional ultrasound conditions were set to Mechanical index (MI) 1.2, Tis 0.6, Freq 4.0/8.0 MHz. Ultrasonic coupling agent was thickly coated as an *in vitro* sound transmission window. The common carotid artery was examined in the anterior followed by the lateral and transverse positions. The internal diameter of the carotid artery and the thickness of the medial membrane and the plaque were measured by local ZOOM. The size of the plaque, internal echo, smooth surface, and ulcer formation was observed, and the video was recorded. All the animal handling procedures and protocols were approved by the Animal Ethics Committee at East China Normal University.

2.2 Hematoxylin-eosin (HE) staining

To evaluate the histological characteristics of atherosclerotic plaques, the left common carotid artery was taken from the rabbit for HE staining. The HE staining was carried out in accordance with standard procedures. The left carotid artery was fixed with 4% formaldehyde and embedded in paraffin. Then, the paraffin-embedded tissue was cut into 5 μm sections. After sealing, a digital microscope was used to observe the pathological changes of the arterial tissue.

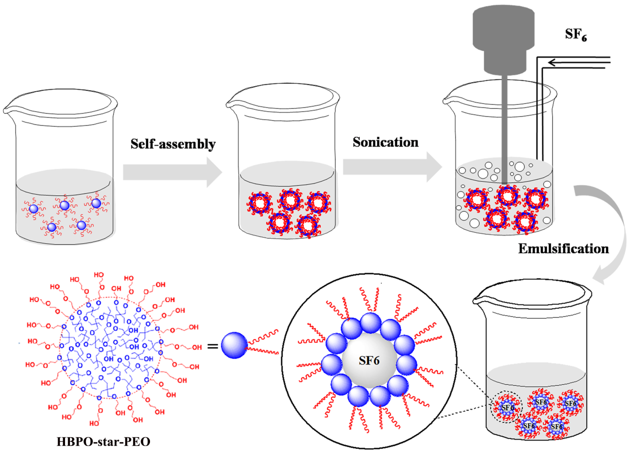

Fig. 1. Schematic diagram of sonic emulsification method. 200 mg of HBPO-star-PEO was added to 10 mL of phosphate buffered saline (10 mL/min) and stirred to dissolve. Sulfur hexafluoride was bubbled into the above solution, and the ultrasound was enhanced with an ultrasonic cell disruptor under ventilation.

2.3 Preparation of nanoscale ultrasonic microbubble contrast agent

Hydrophobic hyperbranched polyether hyperbranched poly(3-ethyl-3-oxetanemethanol) (HBPO) was obtained from a cationic ring-opening polymer using the “one-pot two-step method” [19, 20]. The ring-opening polymerization of ethylene oxide with HBPO was further realized as core to obtain the target product, HBPO-star- poly(ethylene oxide) (HBPO-star-PEO) (Fig. 1). Two hundred mg of HBPO-star-PEO was added to 10 mL of phosphate buffered saline (PBS, Sangon Biotech Co., Ltd., Shanghai, China) and stirred to dissolve. Sulfur hexafluoride (SF6, Shanghai Mi Zheng Gas Co., Ltd., Shanghai, China) was bubbled into the above solution. The ultrasonic cell disruptor conditions for stirring were set under ventilation, as follows: ventilation speed 10 mL/min, temperature 25 °C, pulse 03/01, and amplitude 35% for 2 minutes. Following volume expansion of the original transparent solution, a large amount of density foam appeared, and the solution was kept still for 10 min to obtain cell suspensions containing SF6 [21]. The prepared microbubble suspension was stored at 4 °C for later use. The macromorphology of the nanoscale microbubbles was observed by transmission electron microscopy (TEM, Talos F200, FEI, USA). A dynamic light-scattering (DLS) particle size analyzer (Zetasize Nano ZS90, Malvern, UK) was used to measure the particle size of the nanoscale microbubbles.

2.4 In vivo imaging of nanoscale ultrasonic microbubble contrast agent

The GE Vivid E9 ultrasound scanner (GE Healthcare Co., Milwaukee, Wisconsin, USA) with a line-of-array probe (8–10 MHz) was used for ultrasound examination. The condition was set to MI 1.5 and the image acquisition was performed in the Contrast mode. The peripheral venous channel was established by the ear veins, and the rabbit heart was scaned. First, the rabbit heart was scanned with ultrasound before injecting nano-scale ultrasound microbubbles and the images were recorded. Then, 1 mL of nanoscale ultrasound microbubbles were injected into the heart, and the needle was immediately flushed with 1 mL of saline to observe the perfusion of the heart.

2.5 Preparation of anti-VCAM-1 nanoscale microbubbles and anti-VCAM-1 SonoVue

The VCAM-1 antibody (CAT. No. Ab98954, Abcam, Cambridge, UK) was gradually reacted with the fluorescein isothiocyanate (FITC, ab102884, Abcam, Cambridge, UK) according to the manufacturer's instructions to obtain the FITC/VCAM-1 fluorescence antibody. A PBS buffer was added and diluted to 1 mL, and the 500 uL antibody diluent was absorbed and added into the self-made nanoscale microbubbles suspension, incubated at room temperature for 30 min, the nanoscale microbubbles are floated and the liquid under the nanoscale microbubbles is discarded. The nanoscale microbubbles were washed with the PBS buffer several times until there was clear and transparent in the lower aqueous solution, and the self-made nanobubbles were directly combined with the VCAM-1 antibody to obtain the anti-VCAM-1 nanometer ultrasonic nanoscale microbubbles. Fluorescent reagents and SonoVue microbubbles were mixed to prepare fluorescence-labeled anti-VCAM-1 SonoVue microbubbles. The concentrations of the two types of microbubbles were adjusted to 3×10^8/mL. The fluorescence spectrophotometer LS55, PerkinElmer, Waltham, MA, USA) was used to analyze the antibody carrying capacity.

2.6 Molecular imaging diagnosis of atherosclerosis vulnerable plaque in rabbit carotid artery by self-assembling nanoscale ultrasound microbubble contrast agent

Twenty-five rabbits with carotid atherosclerotic plaques were randomly divided into five groups: Group A (n = 5): injected with 2 mL of the self-made anti-VCAM-1 nanometer ultrasonic microbubble contrast agent; Group B (n = 5): injected with 2 mL of the self-made nanoscale ultrasonic microbubble contrast agent; Group C (n = 5): injected with 2 mL of the anti-VCAM-1 + SonoVue ultrasonic microbubble contrast agent; Group D (n = 5): injected with 2 mL of the SonoVue ultrasonic microbubble contrast agent; Control group (n = 5): injected with 2 mL saline.

The experimental animals were anesthetized and immobilized, and their neck hair was shaved. The GE Vivid E9 ultrasonic diagnostic instrument (GE Healthcare Co., Milwaukee, WI, USA) and 9L linear array probe (8–10 MHz) (GE Healthcare Co., Milwaukee, WI, USA) were used for observation; two-dimensional ultrasound was used to identify the carotid artery before switching to the imaging model (MI 0.14, 0.0, Tis Freq 3.2/6.4 MHz). Contrast agents were injected into the marginal vein of the ear, and the entire contrast-agent filling process was observed and recorded.

To observe the development of the common carotid artery plaque and the lumen enhancement, 4 levels were classified based on the degree of enhancement of the contrast-enhanced ultrasound (CEUS): level I, plaques without enhancement; level II, a dot of enhancement of the plaque; level III, a short linear enhancement of the plaque; level IV, enhancement of plaques throughout or in most parts of the sample.

The CEUS image was exported, and a time-intensity curve was analyzed offline with the EchoPAC software v203 (GE Healthcare Co., Milwaukee, WI, USA). The carotid plaque area was selected as region of interest, and the arrival time, time to peak, basic intensity (BI), peak intensity (PI), and enhancement intensity (EI, EI = PI – BI) were analyzed and compared. The arrival time (in seconds) was defined as the first point of the curve clearly above the baseline intensity, followed by a rise. The time to peak (in seconds) was defined as the time from the start of the injection to the maximum intensity of the curve. The peak intensity (in decibels) was defined as the maximum intensity.

2.7 Immunohistochemical staining

After the experiment, the rabbits were sacrificed, and immunohistochemical staining was performed on the left common carotid artery. The paraffin-embedded tissue was cut into sections with a thickness of 5 μm. The goat serum (no primary antibody) was added to the slices and incubate overnight at 4 °C. Then, a HRP-conjugated goat antimouse IgG (Abcam, Cambridge, MA, USA) as secondary antibody. After the addition of 3, 3′-diaminobenzidine substrate, a digital fluorescent microscope (Olympus, Tokyo, Japan) was used to image the sections.

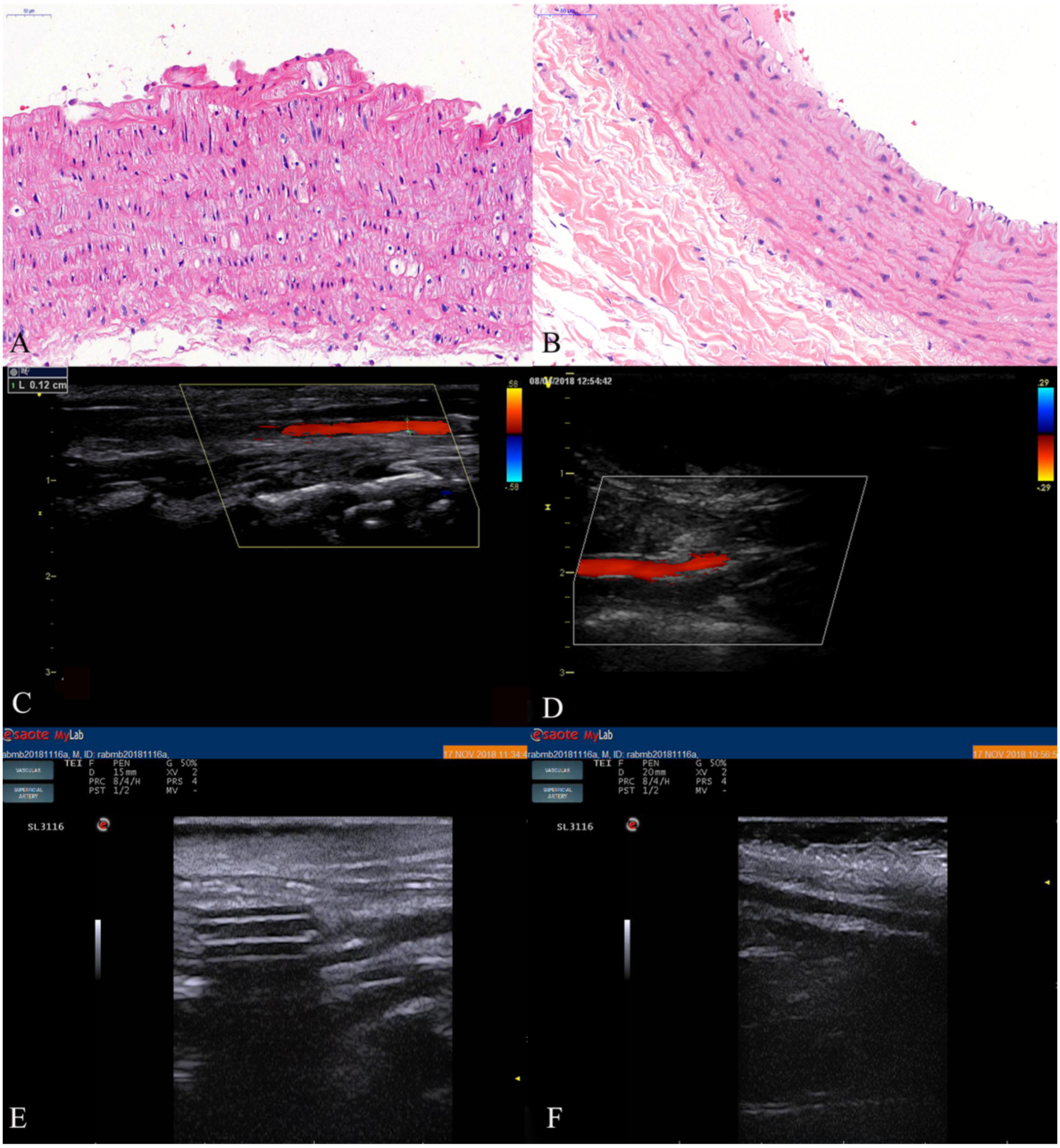

Fig. 2. Formation of vulnerable plaque in rabbit atherosclerosis. (A) HE staining of carotid atherosclerotic plaque in rabbits. (B) HE staining of carotid artery in rabbits of control group (400×). (C,D) Ultrasound images of carotid plaques at 8 weeks showed a slightly hyperechoic mass protruding into the lumen, and the diameter stenosis rate was less than 30%; CDFI showed blood flow. (E,F) Ultrasound images of carotid plaques at 12 weeks. Conventional two-dimensional ultrasonography showed a slightly hyperechoic mass protruding into the lumen on the wall of the common carotid artery, and the diameter stenosis rate was less than 30%.

2.8 Statistical methods

The data were expressed as mean ± standard deviation ($\overline{x} \pm$ S), and were analyzed using SPSS 23.0 software (IBM Corp., Chicago, IL, USA). Two independent sample *t*-tests, one-way analysis of variance or repeated measure analysis of variance were used to compare the differences among groups when appropriate. $p < 0.05$ was considered statistically significant.

3. Results

3.1 Rabbit blood fat detection

Thirty-four rabbits were used to construct rabbit carotid atherosclerotic plaque models, and 25 rabbits were successfully modeled. In 25 rabbits, blood lipid levels increased with feeding time, and the difference of total cholesterol, triglyceride, and low density lipoprotein concentrations between week 8 and 0 was statistically significant (Table 1). There was no statistical difference between week 12 and week 8 (Table 1).

Table 1. Changes of blood lipid concentration and intima-media thickness in rabbits.

	week 0	week 4	week 8	week 12	p-value	p-value
					week 8 vs. week 0	week 12 vs. week 0
TC (mmol/L)	2.36 ± 0.32	6.13 ± 0.41	9.62 ± 0.46*	9.39 ± 0.69	$t = -30.88$, $p < 0.01$	$t = -1.47$, $p = 0.16$
TG (mmol/L)	1.95 ± 0.41	5.86 ± 0.32	9.85 ± 0.69*	10.33 ± 0.78	$t = -40.70$, $p = 0.00$	$t = -0.89$, $p = 0.38$
LDL (mmol/L)	1.70 ± 0.51	5.56 ± 0.39	8.98 ± 0.50*	9.41 ± 0.56	$t = -32.33$, $p = 0.00$	$t = -1.77$, $p = 0.09$
IMT (mm)	0.11 ± 0.01	0.14 ± 0.02	0.38 ± 0.03*	0.52 ± 0.02#	$t = -24.96$, $p = 0.00$	$t = -9.047$, $p = 0.00$

TC, total cholesterol; TG, triglyceride; LDL, Low Density Lipoprotein; IMT, intima-media thickness.

Note: Difference among groups was compared by one-way analysis of variance with. * indicates $p < 0.05$ compared with week 0 and # indicates $p < 0.05$ compared with week 8.

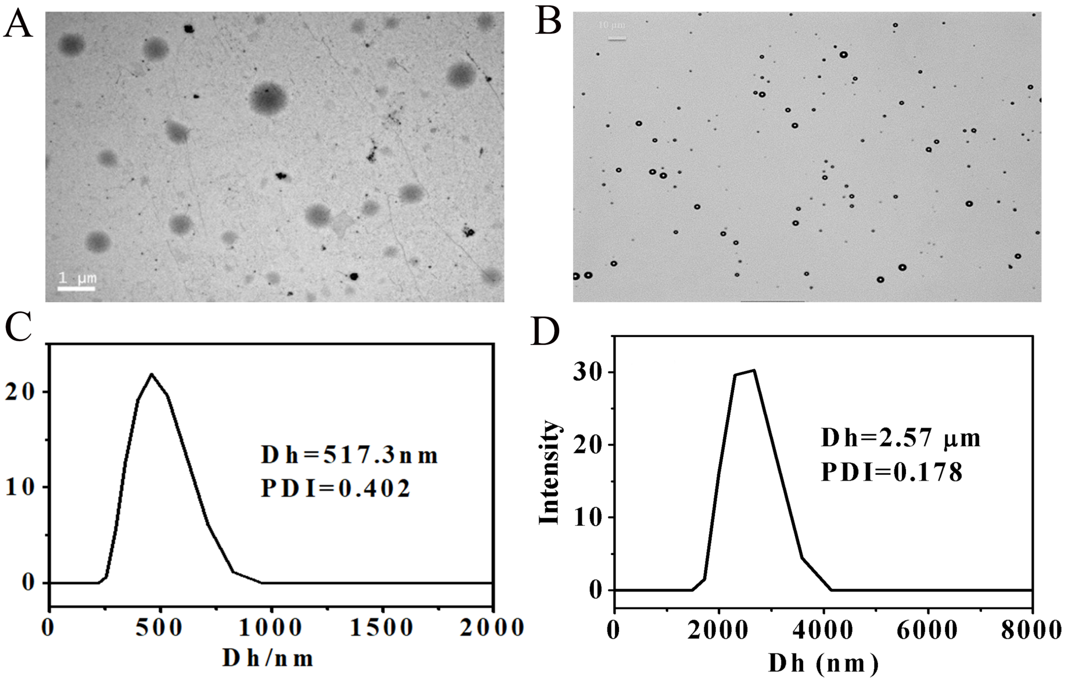

Fig. 3. Self-made microbubble particle size quantitative determination. (A) Self-made microbubble observed by transmission electron microscope. (B) SonoVue microbubble observed by transmission electron microscope. (C) The particle size of the self-made microbubbles is measured by DLS. (D) The particle size of the SonoVue microbubbles is measured by DLS.

3.2 Formation of vulnerable plaque in rabbit atherosclerosis

In order to verify the presence of atherosclerotic plaques, HE staining and contrast-enhanced ultrasound (CEUS) examination were used. In the experimental groups, foam cells were observed under the lesioned intima. The surface fibrous cap structure was broken, the elastic fibers were damaged and thinned, the thickess of media was increased with augmanted smooth muscle cells number and presence of foamy cells, and plaques were observed protruding into the lumen (Fig. 2A). The rabbit endothelial cells in the control group were intact (Fig. 2B).

CEUS showed that the carotid artery intima-media thickness (IMT) was thickened 0.03 mm, and the color Doppler flow signal was well-filled at week 4. At week 8, the carotid artery IMT was thickened more, and some rabbits had small plaques protruding into the lumen. Color Doppler flow imaging (CDFI) showed a filling defect of blood flow at the plaque at the week 8 and week 12, and the diameter stenosis rate was less than 30% (Fig. 2C,D). Compared with the preoperative findings, the difference was statistically significant ($t = 24.96$, $p < 0.01$). Besides, CEUS showed that several rabbits had open collateral vessels and closed common carotid arteries in the cuff, and CDFI showed no blood flow signal in the lumen at week 12 (Fig. 2E,F). The measured values of weekly IMT are shown in Table 1. These results indicate that plaques have formed when the rabbit atherosclerosis model was established.

3.3 In vivo imaging of nanoscale ultrasonic microbubble contrast agent

TEM and DLS data showed that the self-made nanoscale microbubbles have a particle size of about 517.3 ± 73.6 nm, and the SonoVue particle size is 2530.3 ± 163.5 nm (Fig. 3).

Before the contrast agent was injected, the echo signal value inside the heart was very low, and its internal structure cannot be observed (Fig. 4A). After the nano-contrast agent was injected, the rabbit heart was quickly perfused, and

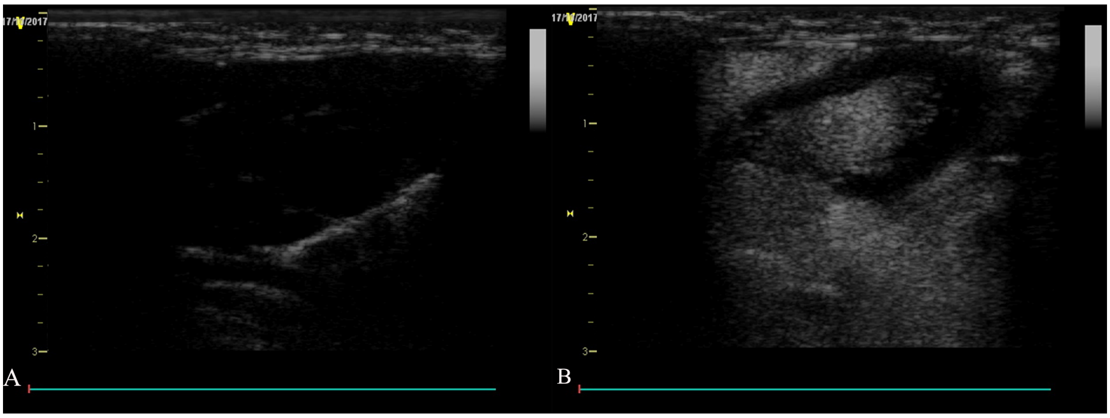

Fig. 4. Rabbit heart radiography. (A) Image before injection of nano microbubbles. (B) Image after injection of nano-microbubbles.

the internal atrioventricular structure and valve activity were clearly visible (Fig. 4B). The average imaging time was 50–60 s, indicating that the self-assembled nanoscale ultrasound microbubble contrast agent hasa certain ability imaging *in vivo.*

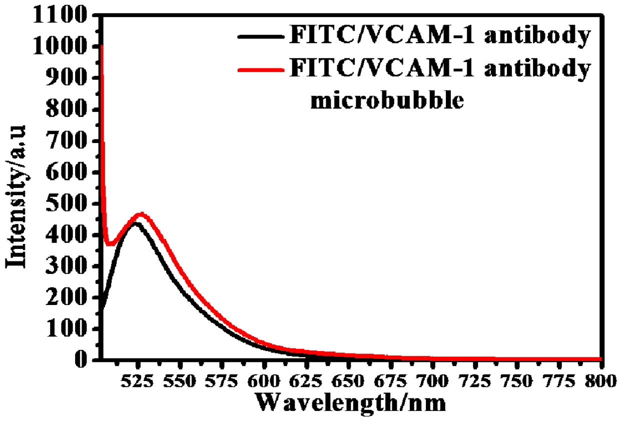

Fig. 5. Quantitative analysis of antibodies carried by microbubbles. VCAM-1 load of the self-made microbubble contrast agent was measured using the fluorescence spectrophotometer.

3.4 Characterization of antibodies carried by nanoscale microbubbles

Under the same determination conditions, the fluorescence intensities of the anti-VCAM-1 with a known fluorescence and the ultrasonic microbubble contrast agent solution with an unknown fluorescence concentration of the VCAM-1 antibody were measured, and the working curve of fluorescence intensity - concentration was drawn. The concentration of the fluorescent anti-VCAM-1 ultrasound microbubble contrast agent was calculated according to the working curve. The antibody loads of the self-made microbubble contrast agent and SonoVue were 3.56 ± 0.13 uL/10^8 microbubbles (Fig. 5) and 0.47 ± 0.07 uL/10^8 microbubbles, respectively.

3.5 Rabbit carotid artery contrast-enhanced ultrasound

After the injection of the ultrasound contrast agent, contrast agent signal was observed in the carotid lumen at 3 seconds after injection in the four groups except for the control group (Fig. 6). The arrival time inside the plaque was later than that of the the carotid lumen, and strengthening began at the plaque base and gradually progressed to the more internal portions or short linear strengthening, which was predominantly level II or level III. After the enhancement lasted for several minutes, the enhancement effect at the plaque gradually weakened, and the contrast agent gradually cleared.

There was a statistically significant difference in the arrival time of the plaques between group A and group B ($p < 0.05$), but there was no statistically significant difference in their time to peak and enhancement intensity (Table 2). However, arrival time, time to peak, and enhancement intensity were not statistically different between group C and group D. Moreover, the arrival time, time to peak and enhancement intensity of the plaques in group A were better than those in group C ($p < 0.05$), and the difference was statistically significant.

3.6 Immunohistochemistry

In order to verify the results of the ultrasound examination, the left common carotid artery of the rabbit was collected and analyzed by immunohistological examination. Immunohistochemical detection results showed that the anti-VCAM-1 nanoscale ultrasound contrast agent group had brown staining of the surface and the internal portions of the carotid plaques. The anti-VCAM-1+SonoVue contrast group also showed minimal dyeing on the surface of the plaques; the other three groups did not express VCAM-1 in the vascular plaque. This indicates that the target ultrasound contrast agent against VCAM-1 may specifically bind to the plaque, and the combined effect of the anti-VCAM-1 nanometer ultrasound contrast agent group was the best (Fig. 7).

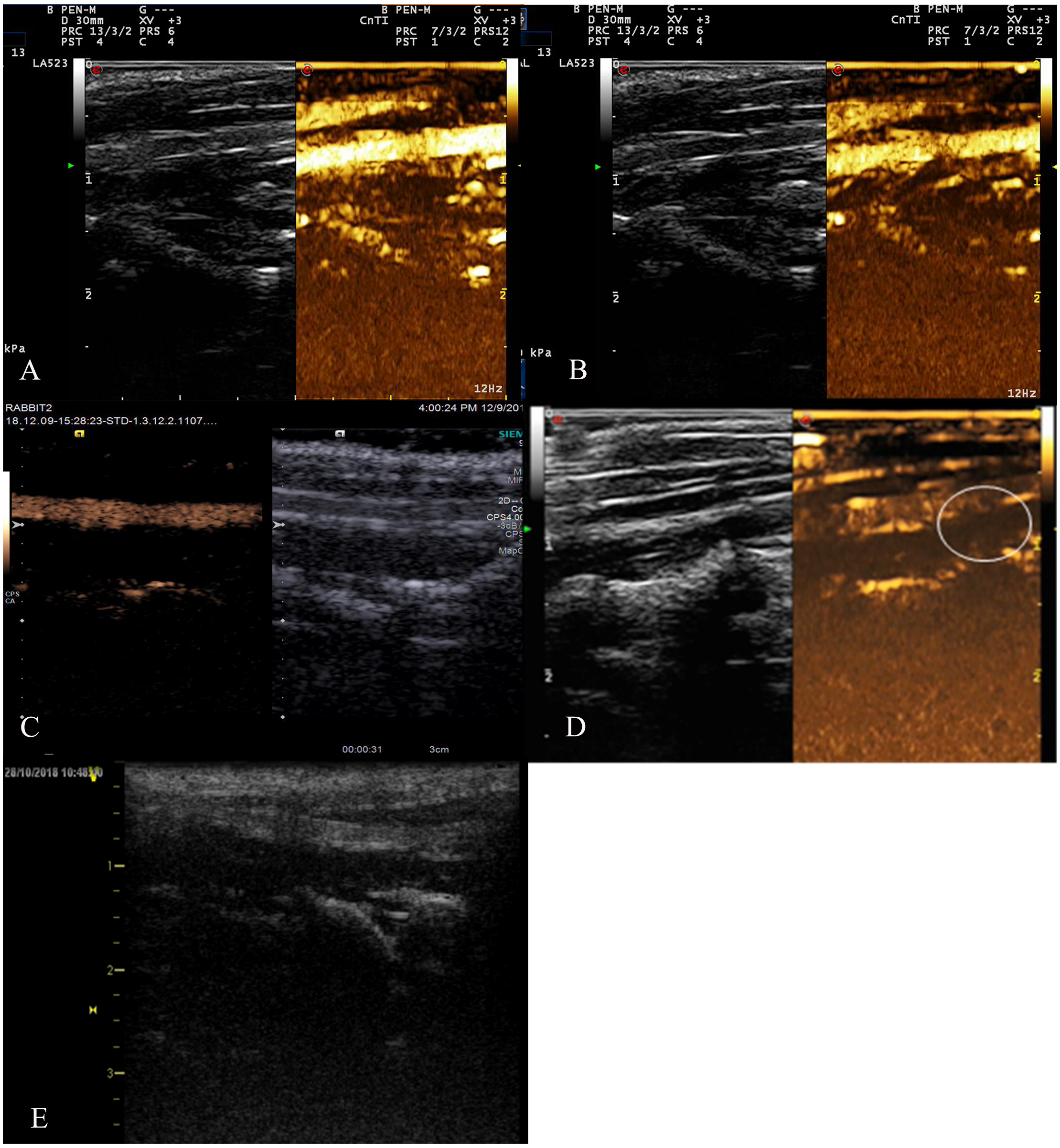

Fig. 6. Rabbit carotid artery contrast-enhanced ultrasound. (A) Image showing the anti-VCAM-1 nanometer contrast agent group with short linear enhancement in the plaque. (B) Image showing the nanoscale contrast agent group with dot enhancement in the plaques. (C) Anti-VCAM-1 sonovi group. (D) SonoVue group; dot enhancement was observed in all plaques. (E) Control group; no contrast agent sonogram is observed in the lumen.

4. Discussion

Atherosclerotic plaque rupture is the main cause of cardiovascular and cerebrovascular events, and the instability and vulnerability of plaques are important risk factors for major adverse cardiovascular events [22, 23]. The mechanism underlying the formation of vulnerable plaques is complex. Studies have found that the inflammatory response is related to the vulnerability of atherosclerotic plaques, and it persists throughout all stages of plaque progression. Plaque inflammation should have occurred in patients in a subclinical state [24, 25]. Neovascularization in atherosclerotic plaque is also a characteristic of vulnerable plaques. When the lipid core of the plaque is hypoxic, macrophages release hypoxic induction factors, which induce neovascularization [26]. Under normal circumstances, the oxygen in the vascular cavity diffuses to the wall of the vessel. When arterial plaque is formed, oxygen cannot diffuse to the adventitia of the blood vessel, and then neovascularization can offset the deficit of oxygen supply and demand [27]. New blood vessels can cause inflammatory cells and lipids to enter the plaque, thicken and enlarge the plaque, and aggravate the narrowing of the arterial lumen. Due to the lack of support from endothelial cells and vascular smooth muscle cells, blood vessels are highly permeable and brittle, and are prone to rupture and bleeding [28]. Therefore, CEUS is important for detecting neovascularization and vascular inflammation during the early stages.

The ideal commercial ultrasound contrast agent should meet the basic requirements of small particle size, long *in vivo*

Table 2. Carotid artery atherosclerotic plaque imaging results.

Group	A	B	C	D	Control	*F*	*p*
Arrival time (s)	9.15 ± 0.12	10.06 ± 0.39	10.93 ± 0.45	10.31 ± 0.41	-	20.67	<0.001
Time to peak (s)	11.23 ± 0.32	11.51 ± 0.39	12.50 ± 0.46	12.33 ± 0.30	-	13.72	<0.001
Enhancement intensity (dB)	11.50 ± 1.37	10.50 ± 1.63	5.99 ± 0.61	6.88 ± 0.70	-	26.78	<0.001

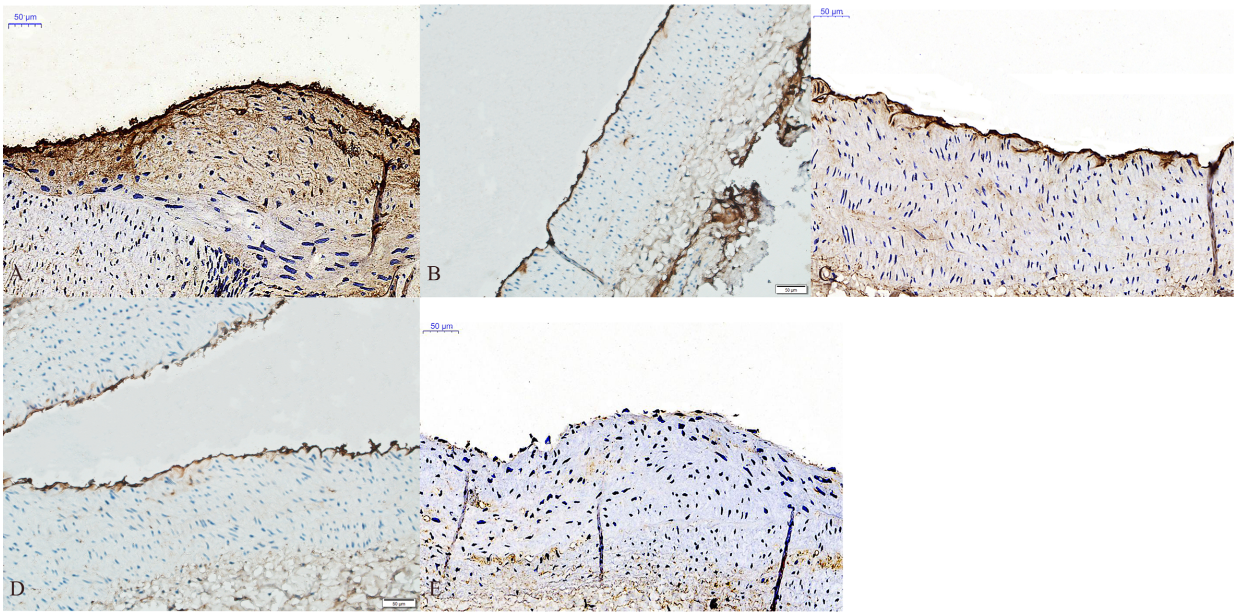

Fig. 7. Immunohistochemical staining. (A) Immunohistochemical staining of plaque in the anti-VCAM-1 nanocontrast agent group. (B) The nanometer contrast agent group. (C) The anti-VCAM-1 SonoVue contrast agent group. (D) The SonoVue contrast agent group. (E) The control group. Magnification 400× in all the panels.

half-life, a soft and elastic shell of the contrast agent, good biocompatibility, and a simple preparation method [29, 30]. With the development of ultrasonic molecular imaging, contrast agents must bind specific antibodies or ligands to become targeted contrast agents. Currently, molecular ultrasound imaging technology based on targeted ultrasound contrast agents has become a research hotspot, and scholars have applied this imaging technology to the evaluation of microvascular endothelial inflammation [31]. With the introduction of new materials, nanoscale ultrasound contrast agents have emerged. Nanoscale ultrasound contrast agents have many advantages over microscale ultrasound contrast agents [32]. First, nanoscale ultrasound contrast agents have stronger penetrating power, and microbubbles with a particle size of <700 nm can easily pass through the enlarged vascular endothelial gap under disease conditions to achieve extravascular imaging. Second, the surface area of nano-microbubbles is relatively large, the adsorption capacity is strong, and it has good biological affinity. Therefore, nanoscale ultrasound contrast agents are good carriers for targeting ligands. Targeting ligands can increase the number of nano-ultrasound contrast agents that accumulate in diseased tissues or organs and increase the effect of contrast imaging. Combining these two technologies has broad application prospects [33]. This study synthesized an anti-VCAM-1 targeting nanoscale ultrasound contrast agent by combining nano-microbubbles with targeting technology.

In previous experiments, we found that the hyperbranched polymer microbubble preparation method was simple; the microbubble could be self-assembled into vesicles in solution. Vesicles of various sizes can be prepared by changing the self-assembly conditions, and the particle sizes can be freely adjusted from nanometers to microns. Self-made vesicles have stable structures and properties similar to those of biofilms [34, 35]. Most importantly, the hyperbranched polymer terminal functional groups are abundant and can serve as binding sites for carrying antibodies or genes [36, 37]. In this study, we prepared microbubbles with a particle size of 517.3 ± 73.6 nm, and we quantitatively determined the antibody load of the microbubbles using a fluorescence spectrophotometer to be 3.56 ± 0.13 uL/10^8, which are higher than those of SonoVue. It is reported that the presence of the contrast agent in the plaque was a sign of neovascularization [38]. When the anti-VCAM-1 targeted contrast agent and the nanocontrast agent were used in rabbits, the point-like or short linear enhancement appears in the plaques. However, the development of the plaque was not significant in the the anti-VCAM-1 SonoVue contrast agent group, the SonoVue contrast agent group and the control group, which may be related to the size of microbubbles.

The arrival time of plaques in the anti-VCAM-1 nanocontrast agent group was earlier than that of the nanocontrast agent group, indicating that the targeting of antibodies can make the microbubbles quickly aggregate to achieve the effect of development. However, there was no statistical difference in the time to peak and enhancement intensity between the anti-VCAM-1 nanocontrast agent group and the nanocontrast agent group. This may be due to the small size of the plaque and the lack of a rich neovascular network inside, so the targeting of microbubbles is not fully expressed.

At present, targeted ultrasound contrast agents have been used to study the cellular and molecular characteristics of ischemia-reperfusion injury, transplant rejection, thrombosis, tumor angiogenesis, and other diseases. Still, they have not been used to target the arterial system with high shear force [39, 40]. The immunohistochemical results of this study showed that the plaques of the anti-VCAM-1 contrast agent group were stained, and it can be concluded that the targeted microvesicles could specifically bind to the VCAM-1 targeted site on the wall of the common carotid artery. This may be because the blood flow in the artery is pulsed, and the diastolic blood flow is relatively slow, which provides a buffer time for the targeted antibody binding target sites and the loading of the contrast agent surface with a large and firm amount of the VCAM-1 antibody [14]. Therefore, the self-made small particle size anti-VCAM-1 targeted ultrasound microbubble contrast agent may be used to diagnose early inflammation of atherosclerotic plaques.

5. Conclusions

In this study, hyperplastic polymer HBPO-STAR-PEo/HBpo-star-PDMAEMA was self-assembled and harmonically emulsified in solution to prepare an ultrasonic contrast agent, with a particle size controlled at 517.3 ± 73.6 nm, and the antibody load is 3.56 ± 0.13 μL/10^8. At the same time, the combination of the self-made microbubble contrast agent and VCAM-1 antibody was simple, and the antibody load was sufficient to target the microvesicles. During *in vivo* contrast imaging, the targeted contrast agent microvesicles attached to the vulnerable plaque of the common carotid artery can significantly improve the development effect of the vulnerable plaque. Therefore, it is feasible to use VCAM-1 antibody on the surface of nano-scale ultrasound microbubble contrast agent to diagnose early inflammation of atherosclerotic plaque.

Author contributions

Conception and design of the research—SLY; acquisition of data—CW, XXC; analysis and interpretation of data—CW, QQH; statistical analysis—CW, KZ, JH; drafting the manuscript—CW; revision of manuscript for important intellectual content—CW, SLY. All authors reviewed the manuscript.

Ethics approval and consent to participate

All the animal handling procedures and protocols were carried out in accordance with relevant guidelines and regulations as well as in accordance with ARRIVE guidelines. All the animal handling procedures and protocols were approved by the Animal Ethics Committee at East China Normal University (Rb20200402).

Acknowledgment

We would like to express our gratitude to all those who helped us during the writing of this manuscript.

Funding

This study was funded by general program of Shanghai Municipal Health and Family Planning Commission (No. 201740053) and the guided project of Shanghai Municipal Science and Technology Commission (No. 18411970000).

Conflict of interest

The authors declare no conflict of interest.

Availability of data and materials

The data analyzed in this study is available from the corresponding author upon reasonable request.

References

[1] Mechtouff L, Rascle L, Crespy V, Canet-Soulas E, Nighoghossian N, Millon A. A narrative review of the pathophysiology of ischemic stroke in carotid plaques: a distinction versus a compromise between hemodynamic and embolic mechanism. Annals of Translational Medicine. 2021; 9: 1208–1208.

[2] Sevuk U, Bahadir MV, Altindag R, Baysal E, Altintas B, Yaylak B, *et al.* Relationship between thyroid function and carotid artery plaque ulceration. Acta Neurologica Belgica. 2015; 115: 581–587.

[3] Kolodgie FD, Yahagi K, Mori H, Romero ME, Trout HH, Finn AV, *et al.* High-risk carotid plaque: lessons learned from histopathology. Seminars in Vascular Surgery. 2017; 30: 31–43.

[4] Nahrendorf M, Sosnovik DE, French BA, Swirski FK, Bengel F, Sadeghi MM, *et al.* Multimodality cardiovascular molecular imaging, Part II. Circulation. Cardiovascular Imaging. 2009; 2: 56–70.

[5] Botnar RM, Ebersberger H, Noerenberg D, Jansen CHP, Wiethoff AJ, Schuster A, *et al.* Molecular imaging in cardiovascular diseases. RoFo. 2015; 187: 92–101.

[6] Vergallo R, Crea F. Atherosclerotic Plaque Healing. New England Journal of Medicine. 2020; 383: 846–857.

[7] van Hinsbergh VWM, Eringa EC, Daemen MJAP. Neovascularization of the atherosclerotic plaque: interplay between atherosclerotic lesion, adventitia-derived microvessels and perivascular fat. Current Opinion in Lipidology. 2015; 26: 405–411.

[8] Van der Veken B, De Meyer GR, Martinet W. Intraplaque neovascularization as a novel therapeutic target in advanced atherosclerosis. Expert Opinion on Therapeutic Targets. 2016; 20: 1247–1257.

[9] Wu JF. Magnetic microbubbles targeted to VCAM-1 for ultrasound molecular imaging of early stage atherosclerosis inflammation. Southern Medical University. 2011. (In Chinese)

[10] Sun J, Liu K, Tang QY, Zhang W, Deng YB. Correlation between enhanced intensity of atherosclerotic plaque at contrast-enhanced ultrasonography and density of histological neovascularization. Journal of Huazhong University of Science and Technology. 2013; 33: 443–446.

[11] Carlos T, Kovach N, Schwartz B, Rosa M, Newman B, Wayner E, *et al.* Human monocytes bind to two cytokine-induced adhesive ligands on cultured human endothelial cells: endothelial-leukocyte adhesion molecule-1 and vascular cell adhesion molecule-1. Blood. 1991; 77: 2266–2271.

[12] Huo Y, Hafezi-Moghadam A, Ley K. Role of vascular cell adhesion molecule-1 and fibronectin connecting segment-1 in monocyte rolling and adhesion on early atherosclerotic lesions. Circulation Research. 2000; 87: 153–159.

[13] Iiyama K, Hajra L, Iiyama M, Li H, DiChiara M, Medoff BD, *et al.* Patterns of vascular cell adhesion molecule-1 and intercellular adhesion molecule-1 expression in rabbit and mouse atherosclerotic lesions and at sites predisposed to lesion formation. Circulation Research. 1999; 85: 199–207.

[14] Wu J, Leong-Poi H, Bin J, Yang L, Liao Y, Liu Y, *et al.* Efficacy of contrast-enhanced us and magnetic microbubbles targeted to vascular cell adhesion molecule-1 for molecular imaging of atherosclerosis. Radiology. 2011; 260: 463–471.

[15] Kaufmann BA, Sanders JM, Davis C, Xie A, Aldred P, Sarembock IJ, *et al.* Molecular imaging of inflammation in atherosclerosis with targeted ultrasound detection of vascular cell adhesion molecule-1. Circulation. 2007; 116: 276–284.

[16] Zheng S, Xu H, Chen H. Nano/microparticles and ultrasound contrast agents. World Journal of Radiology. 2014; 5: 468–471.

[17] Maeda H, Wu J, Sawa T, Matsumura Y, Hori K. Tumor vascular permeability and the EPR effect in macromolecular therapeutics: a review. Journal of Controlled Release. 2000; 65: 271–284.

[18] Xinhua Li, Qidong Yang, Wang Miao, Liu J. Establishment of atherosclerotic plaque Stenosis Model in rabbit carotid artery. Chinese Journal of Practical Nervous Diseases. 2007; 1: 23–25.

[19] Zhou Y, Yan D. Supramolecular self-assembly of giant polymer vesicles with controlled sizes. Angewandte Chemie. 2005; 43: 4896–4899.

[20] Tan H, Li S, Li K, Yu C, Lu Z, Zhou Y. Shape Transformations of Vesicles Self-Assembled from Amphiphilic Hyperbranched Multiarm Copolymers via Simulation. Langmuir. 2019; 35: 6929–6938.

[21] Li J, Huang P, Wang C, Yang SL, Zhou Y. Nano-Scale Ultrasound Contrast Agent Based on Hyperbranched Polyether. Journal of Functional Polymers. 2020; 33: 15–21.

[22] Kataoka Y, Puri R, Nicholls SJ. Inflammation, plaque progression and vulnerability: evidence from intravascular ultrasound imaging. Cardiovascular Diagnosis and Therapy. 2015; 5: 280–289.

[23] Stone GW, Maehara A, Mintz GS. The reality of vulnerable plaque detection. JACC: Cardiovascular Imaging. 2011; 4: 902–904.

[24] Choudhury RP, Fisher EA. Molecular Imaging in Atherosclerosis, Thrombosis, and Vascular Inflammation. Arteriosclerosis, Thrombosis, and Vascular Biology. 2009; 29: 983–991.

[25] Kaufmann BA, Carr CL, Belcik JT, Xie A, Yue Q, Chadderdon S, *et al.* Molecular Imaging of the Initial Inflammatory Response in Atherosclerosis. Arteriosclerosis, Thrombosis, and Vascular Biology. 2010; 30: 54–59.

[26] Nie X, Laforest R, Elvington A, Randolph GJ, Zheng J, Voller T, *et al.* PET/MRI of Hypoxic Atherosclerosis Using 64Cu-ATSM in a Rabbit Model. Journal of Nuclear Medicine. 2017; 57: 2006–2011.

[27] Michel J, Virmani R, Arbustini E, Pasterkamp G. Intraplaque haemorrhages as the trigger of plaque vulnerability. European Heart Journal. 2011; 32: 1977–85, 1985a, 1985b, 1985c.

[28] Sluimer JC, Kolodgie FD, Bijnens APJJ, Maxfield K, Pacheco E, Kutys B, *et al.* Thin-Walled Microvessels in Human Coronary Atherosclerotic Plaques Show Incomplete Endothelial Junctions. Journal of the American College of Cardiology. 2009; 53: 1517–1527.

[29] Zhou Y, Yan D, Dong W, Tian Y. Temperature-responsive phase transition of polymer vesicles: real-time morphology observation and molecular mechanism. The Journal of Physical Chemistry. B. 2007; 111: 1262–1270.

[30] Natfji AA, Ravishankar D, Osborn HMI, Greco F. Parameters Affecting the Enhanced Permeability and Retention Effect: the need for Patient Selection. Journal of Pharmaceutical Sciences. 2018; 106: 3179–3187.

[31] Yan F, Sun Y, Mao Y, Wu M, Deng Z, Li S, *et al.* Ultrasound Molecular Imaging of Atherosclerosis for Early Diagnosis and Therapeutic Evaluation through Leucocyte-like Multiple Targeted Microbubbles. Theranostics. 2019; 8: 1879–1891.

[32] Huynh E, Rajora MA, Zheng G. Multimodal micro, nano, and size conversion ultrasound agents for imaging and therapy. Wiley Interdisciplinary Reviews. Nanomedicine and Nanobiotechnology. 2017; 8: 796–813.

[33] Stride E, Segers T, Lajoinie G, Cherkaoui S, Bettinger T, Versluis M, *et al.* Microbubble Agents: New Directions. Ultrasound in Medicine & Biology. 2020; 46: 1326–1343.

[34] Jin H, Zheng Y, Liu Y, Cheng H, Zhou Y, Yan D. Reversible and Large-Scale Cytomimetic Vesicle Aggregation: Light-Responsive Host-Guest Interactions. Angewandte Chemie International Edition. 2011; 50: 10352–10356.

[35] Dong R, Zhu B, Zhou Y, Yan D, Zhu X. "Breathing" Vesicles with Jellyfish-like on-off Switchable Fluorescence Behavior. Angewandte Chemie International Edition. 2012; 51: 11633–11637.

[36] Jiang W, Zhou Y, Yan D. Hyperbranched polymer vesicles: from self-assembly, characterization, mechanisms, and properties to applications. Chemical Society Reviews. 2016; 44: 3874–3889.

[37] Cheng H, Wang S, Yang J, Zhou Y, Yan D. Synthesis and self-assembly of amphiphilic hyperbranched polyglycerols modified with palmitoyl chloride. Journal of Colloid and Interface Science. 2009; 337: 278–284.

[38] Vicenzini E, Giannoni MF, Puccinelli F, Ricciardi MC, Altieri M, Di Piero V, *et al.* Detection of carotid adventitial vasa vasorum and plaque vascularization with ultrasound cadence contrast pulse sequencing technique and echo-contrast agent. Stroke. 2007; 38: 2841–2843.

[39] Takalkar AM, Klibanov AL, Rychak JJ, Lindner JR, Ley K. Binding and detachment dynamics of microbubbles targeted to P-selectin under controlled shear flow. Journal of Controlled Release. 2004; 96: 473–482.

[40] Luong A, Smith D, Tai C, Cotter B, Luo C, Strachan M, *et al.* Development of a Translatable Ultrasound Molecular Imaging Agent for Inflammation. Ultrasound in Medicine & Biology. 2020; 46: 690–702.